Research Article

Experimental Investigation on Seismic Behaviours of Reinforced Concrete Columns under Simulated Acid Rain Environment

Hao Zheng [ID],[1,2] **Shansuo Zheng** [ID],[1,2] **Yixin Zhang** [ID],[1,2] **Yonglong Cai,**[1,3] **Ming Ming,**[1,2] **and Jingliang Zhou**[1,2]

[1]*School of Civil Engineering, Xi'an University of Architecture and Technology, Xi'an 710055, China*
[2]*Key Lab of Structural Engineering and Earthquake Resistance, Ministry of Education (XAUAT), Xi'an 710055, China*
[3]*Arup, Wuhan 430022, China*

Correspondence should be addressed to Shansuo Zheng; zhengshansuo@263.net and Yixin Zhang; zhangyixin@live.xauat.edu.cn

The purpose of this paper was to systematically investigate the influence of acid rain environments on the seismic behaviour of a reinforced concrete (RC) column. Six RC column specimens with shear span ratios of 2.84 were tested under low cyclic reversed loads after being subjected to accelerated corrosion tests in an artificial climate. The corrosion level and stirrup ratio were used as the control variables. The corrosion ratios of the longitudinal rebars ranged from 0 to 13.17%, and the corrosion ratios of the stirrups varied from 0 to 6.75%. The seismic behaviours of the column specimens were analysed with respect to visual damage, failure mode, hysteresis behaviour, load-carrying capacity, deformation capacity, stiffness degradation, and energy dissipation behaviour. The test results showed that the appearance characteristics of the six column specimens exhibited varying degrees of visual damage as a result of the simulated acid rain exposure. All six specimens were dominated by similar flexural-shear failures under low cyclic reversed loads, regardless of the distinctions in the corrosion levels or stirrup ratios. For the specimens with the same ratios of stirrup, as the corrosion level increased, the load-carrying capacity, deformation capacity, stiffness, and energy dissipation capacity were continuously decreased. For the specimens with the same levels of corrosion, the higher the stirrup ratio was, the stronger the restraint effect of the stirrups on the concrete, and the seismic behaviours of the specimens were obviously improved.

1. Introduction

With economic development and population growth, acid rain pollution has become one of the most intractable environmental issues in many countries and regions [1, 2]. Furthermore, acid rain tends to spread and worsen [3–5]. Acid rain not only threatens natural ecology but also has a significant influence on building structures. It is well known that acid rain exposure is one of the primary durability issues for reinforced concrete (RC) structures, and acid rain exposure leads to the deterioration of the mechanical properties of concrete, such as its compressive strength and elastic modulus [6, 7], and to the corrosion of steel bars [8]. Over time, the reliability of an RC structure in an acid rain environment gradually decreases; hence, it is of great

importance to conduct in-depth and systematic research on the seismic behaviours of RC structures exposed to acid rain.

The influence of acid rain on the material-level behaviours of concrete has been a popular issue for the past few years, including studies on surface morphology [9], corrosion mechanism [10–13], damage testing method [6], compressive strength [6, 14], elastic modulus, and fracture toughness [15, 16]. Hill et al. [9] reported that spalling and crushing of concrete cube specimens caused by sulfate and acid exposure initially appeared at the corners and edges of the specimens. Light optical microscopy combined with chemical analysis was used by Gregerová and Všianský [10] to detect corrosion products of concrete under sulfuric acid exposure. In addition, they believed that the deterioration of the macroscopic mechanical properties of concrete was

essentially caused by the accumulation of microscopic damage. Xie et al. [11] carried out an accelerated corrosion test by using a mixed solution of sulfuric acid, nitric acid, and ammonium sulfate to simulate the various deterioration stages of cement concrete specimens during acid rain exposure. The corrosion of concrete by a simulated acid rain solution was divided into three stages; the neutralization depth of specimens can be expressed as a function of the corrosion time; and the deterioration of material properties of specimens was caused by H^+ dissolution damage and SO_4^{2-} expansion damage. Chen et al. [12] also noted that the degradation of the mechanical properties of concrete cementitious specimens subjected to simulated acid rain exposure resulted from the coupled effect of H^+ and SO_4^{2-}, and the deterioration accumulated from the outside to the inside of the specimens. Okochi et al. [13] experimented with the influence of acid deposition on a concrete structure by using an indoor spray test and a field exposure test. Their results showed that the higher the concentration of H^+ and SO_4^{2-} was, the more severely the concrete was corroded. Fan et al. [6] conducted a range of tests on 354 concrete prismatic samples with dimensions of $150 \, mm \times 150 \, mm \times 300 \, mm$. Ultrasonic testing technology was a reliable method for the nondestructive measurement of damage depth, and the damage index corresponding to the change in the relative compressive strength was more suitable for characterizing the deterioration state of concrete exposed to acid rain. Zha and Lu [14] investigated the differentiae, on account of experimental research, in the compressive strengths of ordinary Portland concrete and recycled concrete under artificial acid rain exposure. Under the action of a simulated acid rain exposure, significant variations occurred in the physical and chemical properties of the concrete material, resulting in a corresponding reduction in fracture toughness and elastic modulus, and the lower the pH value, the faster the degradation rate [15, 16].

Conclusively, the deterioration of the mechanical properties of concrete caused by acid rain exposure has been fully studied. On the component level, acid rain exposure not only influences the mechanical properties of concrete but also corrodes the internal steel bars. Less attention has been devoted to the variations in the mechanical properties of RC components subjected to acid rain exposure. Guan and Zheng [8] employed an artificial climate simulation technology to study the effect of acid rain on the seismic behaviours of interior beam-column joints with different axial compression ratios. An artificial rainfall device was designed by Fan et al. [17] to simulate real acid rain, and the flexural behaviours of RC beams operating in an acid rain environment were investigated. Hence, the surface morphology and mechanical properties of RC components were significantly affected by acid rain.

RC columns are the main load-carrying components in an RC structure, wherein the columns carry the loads from beams and slabs and further transfer the loads to the foundation [18]. If some columns failed during an earthquake, the reliability of the whole structure would be greatly adversely affected. An RC column component under an acid rain environment is subjected to the corrosive media of carbon dioxide, sulfate ions, and nitrate ions. As a result, the overall mechanical properties and seismic behaviours of an RC column component are constantly deteriorated each day, which gravely threatens the reliability of an in-service RC building structure. However, for RC columns, the existing research has focused only on the effects of steel bar corrosion on the behaviours of RC columns. Based on simulated seismic loading tests of eight full-size corroded RC short columns, Vu and Li [19] found that the shear strengths and deformation capacities of corroded columns were markedly lower than those of noncorroded columns, particularly under high corrosion levels and high axial compression ratios. Moreover, methods considering the influence of stirrup corrosion for evaluating the shear strength of short concrete columns were proposed. Ma et al. [20] conducted quasistatic loading tests on thirteen circular RC columns that had been subjected to accelerated corrosion tests. On the strength of the test results, degradation models of seismic performance indicators involving the strengths and ductilities of columns were presented. Li et al. [21] analysed the impact of nonuniform steel bar corrosion on the seismic performance of RC columns. Under the influence of nonuniform steel bar corrosion, the seismic performance of RC columns after peak points was dramatically diverse in the positive and negative loading directions. In the experimental study performed by Meda et al. [22], it was reported that the load-bearing and deformation capacities of RC columns under cyclic loading were substantially influenced by the corrosion of the reinforcement. Li et al. [23] experimented with the cyclic behaviours of eight RC columns with corroded stirrups. Their results showed that the bearing capacities of columns increased slightly at the outset when the corrosion ratios of the stirrups were less and then decreased as the corrosion ratio increased further. Yang et al. [24] investigated the bending capacities of corroded RC columns, which simulated a marine environment. The hysteretic behaviours of columns deteriorated as the corrosion level increased. For example, when the maximum mass loss ratio of the reinforcing bars reached 16.8%, the bending strength and ductility coefficient of the corroded column were reduced by 20% and 32.1%, respectively, compared with those of the column without corrosion. In the above analyses, electrochemical methods were adopted to accelerate the corrosion processes of steel bars in RC columns, and many achievements were made. Nevertheless, as far as the authors know, the study on the seismic behaviours of RC columns corroded by such corrosive media as carbon dioxide, sulfate ions, and nitrate ions in an acid rain environment has not been reported to date.

In view of the above accounts, this paper aims to experimentally study the influence of the corrosion level, which is regulated by an artificial climate accelerated corrosion technique, on the seismic behaviours of RC columns under an acid rain environment. In this test, six RC column specimens were fabricated with different corrosion levels and stirrup ratios, and the columns were subjected to low cyclic reversed loads. The test outcomes are conducive to the evaluation of seismic behaviours for RC structures damaged by acid rain.

2. Experimental Programme

2.1. Specimen Details. Six RC column specimens were designed and made in accordance with the regulations of Chinese codes [25–27]. The corrosion level and stirrup ratio were the controlled variables in the experiments. The axial compression ratios of all the six specimens were 0.3. The geometric dimensions and steel bar layout of the six column specimens are presented in Figure 1. The cross sections ($b \times h$) and heights of all columns were 200 mm × 200 mm and 600 mm, respectively, which produced the same shear span ratio of 2.84. The thicknesses of the concrete covers were 10 mm. The longitudinal rebars were symmetrically collocated, i.e., three 16 mm diameter deformed bars (grade HRB335) were equipped on each side. In addition, 6 mm diameter round bars (grade HPB300) were employed for the stirrups. The geometries of the foundation beams were 1000 mm × 400 mm × 400 mm. The main test parameters of the column specimens are summarized in Table 1. Note that the focus of this paper is limited to the seismic behaviours of RC columns with shear span ratios of 2.84 under a simulated acid rain environment. Moreover, the test outcomes of the influence of acid rain on RC columns with shear span ratios of 5.68 will be reported later.

The strength grade of the concrete was C40, which was formulated with Portland 42.5R cement. The mix composition was 500 kg/m^3 for cement, 559 kg/m^3 for sand, 1136 kg/m^3 for fine gravel, and 205 kg/m^3 for water. Twelve cubes with dimensions of 150 mm × 150 mm × 150 mm were cast in addition to the column specimens and were divided into four groups of three cubes each. The four group cubes were subjected to 0, 240, 360, and 480 spray cycles, respectively. The mean compressive strengths of the concrete cubes were tested. The results are reported in Table 2. Furthermore, the measured mechanical properties of the steel bars are provided in Table 3.

2.2. Simulated Acid Rain in the Environmental Chamber. In recent years, artificial climate accelerated corrosion techniques have been continuously developed and extensively employed in durability testing research of RC structures [8, 28–30]. The Model ZHT/W2300 environmental chamber at Xi'an University of Architecture and Technology was used to perform accelerated corrosion tests with an artificial climate accelerated corrosion technique on column specimens, wherein the environmental parameters (temperature, humidity, and spray solution duration) were set in the chamber, as shown in Figure 2.

It should be noted that a secondary casting method of separating foundation beams from columns is adopted to prevent the failure mode of column specimens from transforming, which might be affected by the corrosion of foundation beams. The columns were first cast and naturally cured for 28 days. Afterward, the steel bars located at the bottom of columns were sealed with epoxy resin, and the columns were placed into the chamber for the accelerated corrosion tests. The columns and foundation beams were recast together right after the preset spray cycles were finished.

The confecting scheme of the simulated acid rain solution referenced the works of Xie et al. [11] and Chinese meteorological data [31]. First, to preliminarily form the solution, sodium sulfate (Na_2SO_4) was added to tap water until the concentration of sulfate ions in the solution reached 0.06 mol/L. Subsequently, nitric acid (HNO_3) with a concentration of $\rho = 1.42$ g/cm^3 was added to the solution to adjust the pH value of the solution to 3.0. The specific corrosion scheme is listed as follows: (a) The chamber temperature was adjusted to $25 \pm 5°C$, and the simulated acid rain solution was sprayed for 240 min. (b) The temperature was increased to $65 \pm 5°C$ at a constant speed, and then specimens were dried for 96 min. (c) The temperature was decreased to $25 \pm 5°C$ at a constant speed, and a new spray cycle was conducted. As described, each spray cycle took 360 min, as shown in Figure 3.

The corrosion level of the specimens is governed by presetting the number of spray cycles (0, 240, 360, and 480), as presented in Table 1. Column SC-1 was used as the control, and no corrosion test was performed on this column.

In this paper, the precipitation intensity of a certain city was used to control the period of the simulated acid rain exposure in the laboratory [17, 32, 33]. Chongqing, which is one of China's largest cities and suffered severe acid rain exposure, was taken as the research object, and its annual average precipitation intensity is about 1100 mm/a [34]. During the accelerated corrosion tests, the precipitation intensity in the laboratory was set to 34.5 mm/h, that is, the number of spray cycles of 240, 360, and 480 in Table 1 corresponded to the precipitation in Chongqing for 30, 45, and 60 years, respectively.

2.3. Test Setup. The schematic diagram of the test setup is illustrated in Figure 4. Linear variable differential transformers (LVDTs) were mounted to monitor the lateral displacements of the specimens. One LVDT was located at the loading point to measure the lateral displacement of the column top. Another LVDT was mounted on the axis of the foundation beam to measure its lateral slip. In addition, two additional pairs of LVDTs were used for measuring shear displacements and rotations in the plastic hinge areas where the length was evaluated as 170 mm [35]. To simulate the actual load conditions of RC columns under earthquake excitation as accurately as possible, low cyclic reversed loading tests were conducted on the designed RC column specimens by cantilever loading. Concurrently, the specimens were fixed to the strong floor by anchoring screws throughout testing processes. Vertical loads were applied by a hydraulic jack with a capacity of 1000 kN. Lateral low cyclic reversed loads were applied by an electrohydraulic servo actuator with a capacity of 500 kN that was fixed on the reaction wall. Lateral push-pull displacements were controlled by a sensor.

The lateral loading procedure was performed in accordance with displacement-controlled steps after the preadded
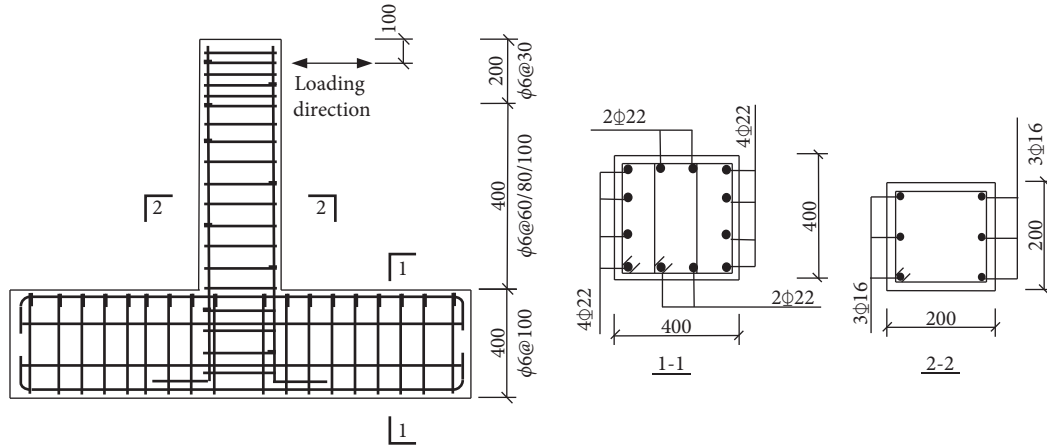
Figure 1: Geometric dimensions and steel bar layout of the column specimens (unit: mm).

Table 1: Main test parameters of the column specimens.

| Specimen | Stirrup | Simulated acid rain solution | | Number of spray cycles | Acidification depth |
		Value of pH	Concentration of SO_4^{2-} (mol/L)		
SC-1	φ6@60	/	/	0	/
SC-2	φ6@60	3.0	0.06	240	6.12
SC-3	φ6@60	3.0	0.06	360	7.08
SC-4	φ6@60	3.0	0.06	480	8.32
SC-5	φ6@80	3.0	0.06	480	8.17
SC-6	φ6@100	3.0	0.06	480	8.43

Table 2: Mechanical properties of the concrete cubes.

Number of spray cycles	Cubic compressive strength (MPa)
0	45.3
240	45.1
360	43.5
480	40.3

Table 3: Mechanical properties of the steel bars.

Diameter (mm)	Yielding strength (MPa)	Ultimate strength (MPa)	Elastic modulus (MPa)
φ6	305	440	2.1×10^5
φ16	373	537	2.0×10^5

reciprocating load was implemented twice [25]. When the residual lateral load of a specimen was reduced to 85% of the peak load, the loading was stopped. The loading protocol is given in Table 4.

3. Experimental Observations

3.1. Visual Damage under Simulated Acid Rain. The visual damage to the specimens, which had been accomplished by the preset spray cycles, was evaluated, as shown in Figure 5. It was found that there were noticeable differences in the visual damage of specimens under different corrosion levels, and the visual damage was continuously exacerbated by increasing the corrosion level.

The control column, SC-1, had a uniform concrete colour, smooth and flat surfaces, and defined corners, as shown in Figure 5(a).

The face of column SC-2, which was subjected to 240 spray cycles, was partially yellowed and accompanied by white crystal precipitates, as shown in Figure 5(b). In this period, H^+ in the simulated acid rain solution chemically reacted with concrete to form a small amount of $CaSO_4 \cdot 2H_2O$ crystals covering the concrete surface. In addition, chemical reactions led to the decomposition of hydration products on the surface of the column. These phenomena indicated that acid rain caused significant corrosion on the concrete surface in the early period of the accelerated corrosion process.

As the number of spray cycles increased to 360, sand, voids, and pitting were observed on the surface of column SC-3, and the texture of the concrete became loose, as shown in Figure 5(c). This might ascribe to the formation and expansion of $CaSO_4 \cdot 2H_2O$ and Aft, the dissolution of aggregates, and a continuous variation in the contents of the hydration products such as $Ca(OH)_2$, hydrate calcium silicate (C–S–H) gel, $xCaO \cdot Al_2O_3 \cdot yH_2O$ (C_xAH_y), and $xCaO \cdot Fe_2O_3 \cdot yH_2O$ in concrete due to chemical reactions.

As the number of spray cycles increased to 480, the surface of column SC-4 was rougher than those of the other columns, and a peeling phenomenon was observed on the surface of the concrete. In addition, the texture of the concrete became looser than that of SC-4, and certain exposed coarse aggregates could also be observed, as shown in

(a) (b)

FIGURE 2: Photographs of the environmental chamber. (a) Exterior. (b) Interior.

FIGURE 3: Corrosion scheme in the environmental chamber.

FIGURE 4: Setup for the loading tests. (1) Column specimen; (2) reaction wall; (3) hydraulic actuator; (4) lateral load transfer assembly; (5) hydraulic jack; (6) sliding support; (7) reaction beam; (8) sensor; (9) LVDTs; (10) anchoring screws; (11) foundation beam; (12) strong floor; (13) gantry.

TABLE 4: Loading protocol.

Loading level	Δ_1	Δ_2	Δ_3	Δ_4	Δ_5	Δ_6	Δ_7	Δ_8	Δ_9	Δ_{10}	Δ_{11}	Δ_{12}	Δ_{13}	Δ_{14}	Δ_{15}	Δ_{16}	Δ_{17}	Δ_{18}
Displacement (mm)	0.3	0.6	0.9	1.2	1.5	1.8	2.4	3.3	3.9	4.5	5.0	6.5	8.0	10.0	13.0	16.0	19.0	22.0
Number of cycles	1	1	1	1	1	1	1	3	3	3	3	3	3	3	3	3	3	3

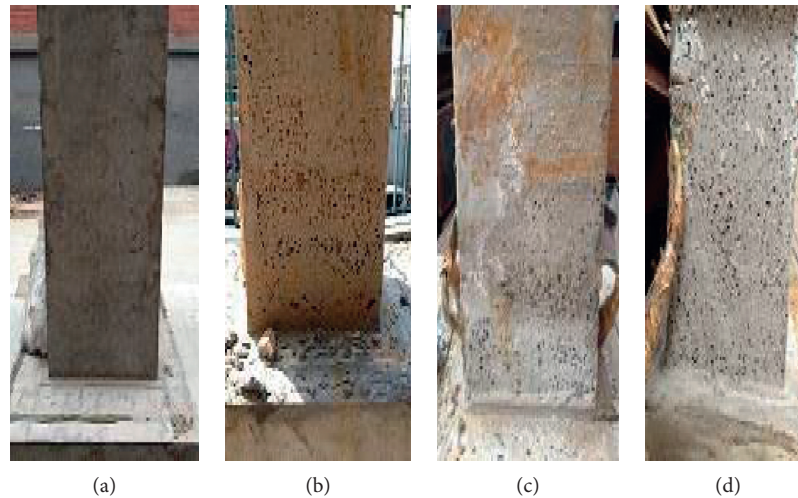|			
(a)	(b)	(c)	(d)

FIGURE 5: Visual damage of specimens under different levels of corrosion: (a) SC-1 (0 cycles); (b) SC-2 (240 cycles); (c) SC-3 (360 cycles); (d) SC-4 (480 cycles).

Figure 5(d). The reason why is that corrosion products such as $CaSO_4 \cdot 2H_2O$ and Aft were continuously produced during this period. Furthermore, the dissolution of aggregates and the decomposition of hydration products were more serious.

The visual damage for the appearance characteristic of columns SC-4, SC-5, and SC-6 was similar.

3.2. Acidification Depth.

The acidification depth is the penetration depth in concrete material attack by acidic material in simulated acid rain solution [15, 36, 37]. The acidification depth was utilized in this paper to evaluate the acidification evolution of the specimens subject to simulated acid rain exposure, which characterized the corrosion damage extent of the specimens.

Table 1 summarizes the variation of acidification depth of the specimens over the number of spray cycles. The acidification depth of the specimens increased nonlinearly with the number of spray cycles. The acidification process can be approximately divided into two stages, namely, initial growth period and stable growth period. In the initial growth period, since the cement hydration products were alkaline, once they contacted the acid solution, the neutralization reaction occurred immediately. The acidification rate was fast in this period. After 240 spray cycles, the acidification depth of the specimen was 6.12 mm. Then, in the stable growth period, as a result of the formation and expansion of corrosion products (such as $CaSO_4 \cdot 2H_2O$ and Aft), the original pores in the concrete were filled, and the surface area of the specimen became dense. The generated corrosion products acted as a protective layer, delaying the further acidification process of acidic material to inside concrete of the specimen. The acidification rate slowed down in this period. After 360 and 480 spray cycles, the acidification depth of the specimen increased to 7.08 and 8.17~8.43 mm, respectively.

3.3. Damage Process and Failure Mode.

The ultimate crack patterns and failure morphologies of the six column specimens are shown in Figure 6. All column specimens were dominated by similar flexural-shear failures under low cyclic reversed loads. The typical failure process and damage characteristics are described as follows. Before the longitudinal rebars yielded, horizontal bending cracks were first observed at the column base. Subsequently, a few tiny vertical compression cracks, which were visible to the naked eye, emerged along the longitudinal rebars at four corners of the column. As the loading displacement amplitude increased, the present vertical compression cracks continued to extend upward. The original horizontal bending cracks broadened continuously, and certain parts of these cracks propagated obliquely. In addition, a plurality of intersecting flexural-shear cracks gradually appeared at the bottom of the column, which indicated that the shearing effect was enhanced in the column. With the further increase in the loading displacement amplitude, the longitudinal rebars started to yield, and the stirrups intersecting the flexural-shear cracks were approaching their tensile yielding strengths. Thereafter, the number of diagonal cracks did not increase further; however, the lengths and widths of these cracks continued to increase. The concrete cover on the frontage, within 0~200 mm from the bottom of the column, was crushed in stages and increasingly peeled off. The test ended when the remaining lateral load of the column decreased to 85% of the peak load. Eventually, the dominant diagonal shear cracks with long and wide extensions were formed in the lower part of the column at failure. A tortoise-shaped surface and a large spalled area were observed on the concrete of the lower part of the column, and a portion of exposed steel bars was also observed.

The failure processes and damage characteristics of the columns showed a certain discrepancy due to the variation in the corrosion levels and stirrup ratios, which could be discussed as follows:

(1) For columns SC-1, SC-2, SC-3, and SC-4 with the same stirrup ratios, as the level of corrosion increased, the number of cracks in the lower parts of

Figure 6: Ultimate crack patterns and failure morphologies of the specimens: (a) SC-1; (b) SC-2; (c) SC-3; (d) SC-4; (e) SC-5; (f) SC-6.

the columns decreased, whereas the crack spacing increased and the crack width broadened. The reason for these phenomena is that the corrosion of the steel bars weakened the bonding properties between the steel bars and the surrounding concrete, which led to the required transmission path increasing when a load of steel bars was transmitted to the concrete by means of the shear bond strength, thereby increasing the crack spacing. Moreover, the crack width is proportional to the crack spacing; thus, the crack width broadened by increasing the crack spacing.

(2) For columns SC-4, SC-5, and SC-6 with the same corrosion levels, as the stirrup ratio increased, X-shaped flexural-shear cracks in the plastic hinge area of columns formed later and propagated more slowly. This finding indicated that the shear failure characteristics of the columns

became less apparent at the end of the tests; therefore, the columns were less vulnerable to earthquake action.

4. Experimental Results and Discussion

4.1. Corrosion Ratio of the Steel Bar. The corrosion of the steel bars in the plastic hinge area of an RC column is one of the main reasons for the deterioration of the seismic behaviour of the column. Therefore, steel bars, in the range of 300 mm at the bottom of columns, were marked during casting. After the loading tests ended, the concrete covers in the plastic hinge area of columns were first smashed, and the longitudinal rebars and stirrups in the marked area were separately removed. Hereafter, the concrete and rust products adhering to these removed steel bars were cleared. Afterward, the surfaces of these steel bars were cleaned with hydrochloric acid with a mass concentration of 12% and

rinsed with water successively and then neutralized with limestone. Finally, these steel bars were placed in an electric oven for approximately 4 hours to dry, and then the bars were weighed by a balance. The corrosion ratio, which reflects the actual corrosion condition of a steel bar, is calculated as follows:

$$\eta = \frac{m_1 - m_0}{m_0}, \quad (1)$$

where η is the actual corrosion ratio of the steel bar in terms of mass loss ratio; m_0 is the weight of a unit length of the noncorroded steel bar; and m_1 is the weight of a unit length of the corroded steel bar after descaling.

There was still a certain degree of diversity in the actual mass loss ratios of these steel bars, even under the same corrosion level. Consequently, the average mass loss ratio of the longitudinal rebars and stirrups for each column was taken as the actual corrosion ratio of the longitudinal rebar and stirrup, respectively. The calculation results are summarized in Table 5.

These results indicated that the corrosion ratios of the longitudinal rebars and the corrosion ratios of the stirrups were accelerated by increasing the corrosion level, and the relationships were both approximately linear. With the same number of spray cycles, the corrosion ratio of a stirrup was significantly greater than that of a longitudinal rebar. The main reasons for this phenomenon are illustrated as follows. On the one hand, with the same corrosion depth, the smaller the diameter of a steel bar is, the greater the calculated corrosion ratio is, while the diameter of a stirrup in the columns was indeed smaller than that of a longitudinal rebar. On the other hand, the distance between the stirrups and the outer surface of concrete is small. When a corrosive medium reached the surfaces of the stirrups and led to corrosion, the longitudinal rebars have not yet been affected by the corrosive medium.

4.2. Hysteresis Behaviour. The hysteresis loop is the interrelation of the lateral load and the top lateral displacement, which can reflect the force state and deformation procedure of a specimen throughout the loading process. Figure 7 displays the hysteresis loops of the six column specimens.

(1) The hysteresis loops of the specimens exhibited the following analogous features. Prior to the yielding point, the hysteresis loop was approximately linear, and the loop was minuscule; therefore, there was no significant variation in the stiffness during loading and unloading, and there was almost no residual deformation at the end of the unloading routes. As the loading displacement amplitude increased, the longitudinal rebars in the specimens began to yield, and the form of the hysteresis loop translated from approximately linear to shuttle-shaped. The stiffness during loading and unloading was degraded with each subsequent stage, the bearing capacity was steadily improved, and obvious residual deformation was observed. Moreover, the area enclosed by the hysteresis loop expanded, which showed evidence of

TABLE 5: Corrosion ratios of the steel bars.

Specimen (%)	SC-1	SC-2	SC-3	SC-4	SC-5	SC-6
η_l	0	2.53	4.54	6.75	5.86	6.23
η_s	0	5.32	8.13	11.46	12.77	13.17

Note: η_l and η_s are the corrosion ratios of the longitudinal rebars and stirrups, respectively.

great energy dissipation for the specimens in this stage. After reaching the peak point, the hysteresis loop exhibited a considerable pinching effect. Simultaneously, the loop converted to an inverted S-shape and gradually reduced in size. The stiffness degradation was further exacerbated due to the formation and expansion of inclined cracks in the lower parts of the specimens.

(2) With respect to columns SC-1, SC-2, SC-3, and SC-4 under the same stirrup ratios and different corrosion levels during the initial stage of loading, the hysteresis loops varied linearly, and the slopes of the loops decreased slightly as the corrosion level increased. Thereafter, as the level of corrosion increased, the platform segment near the peak point became shorter. Moreover, the pinching effect of the hysteresis loops became increasingly obvious, leading to a progressive reduction in the fullness and area of each loop at the same displacement-controlled loading level. After the lateral load reached the peak value, the greater the level of corrosion was, the faster the slopes of the load-displacement curves reduced, and the quicker the load-carrying capacities of specimens degraded.

(3) With respect to columns SC-4, SC-5, and SC-6 under the same corrosion levels and different stirrup ratios, before the lateral loading displacement reached the displacement value of the peak point, the form of the hysteresis loop for column SC-4 was nearly the same as those of SC-5 and SC-6, whereas the strength attenuation and stiffness degradation of SC-4 were relatively insubstantial at the same displacement-controlled loading level. After the lateral loading displacement reached the displacement value of the peak point, the rate of size reduction in the hysteresis loop for column SC-4 was less than those for SC-5 and SC-6, indicating the stronger energy dissipation behaviour of SC-4. Moreover, the displacement corresponding to the ultimate point of column SC-4 was larger than those of SC-5 and SC-6, i.e., the ductility of SC-4 was relatively better than that of the other columns. This phenomenon is because a higher stirrup ratio could effectively restrict the extension of the cracks and delay the buckling of the longitudinal rebars, which provides excellent load-carrying and deformation capacities to an RC column.

4.3. Skeleton Curve. Figure 8 shows the skeleton curves of the six column specimens, which were designated as the averages of the maximum absolute values of the load and
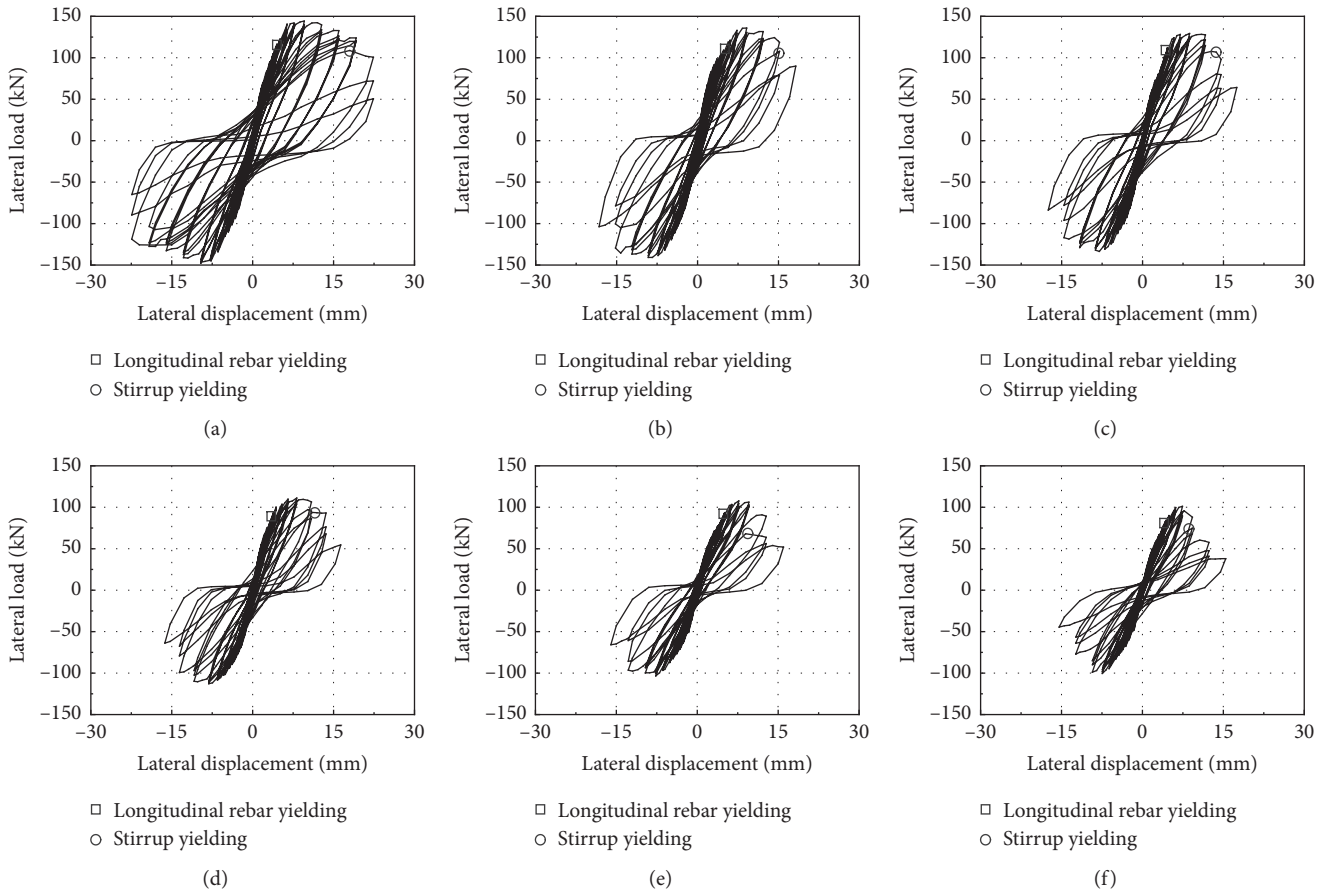
Figure 7: Hysteresis loops of the specimens: (a) SC-1; (b) SC-2; (c) SC-3; (d) SC-4; (e) SC-5; (f) SC-6.
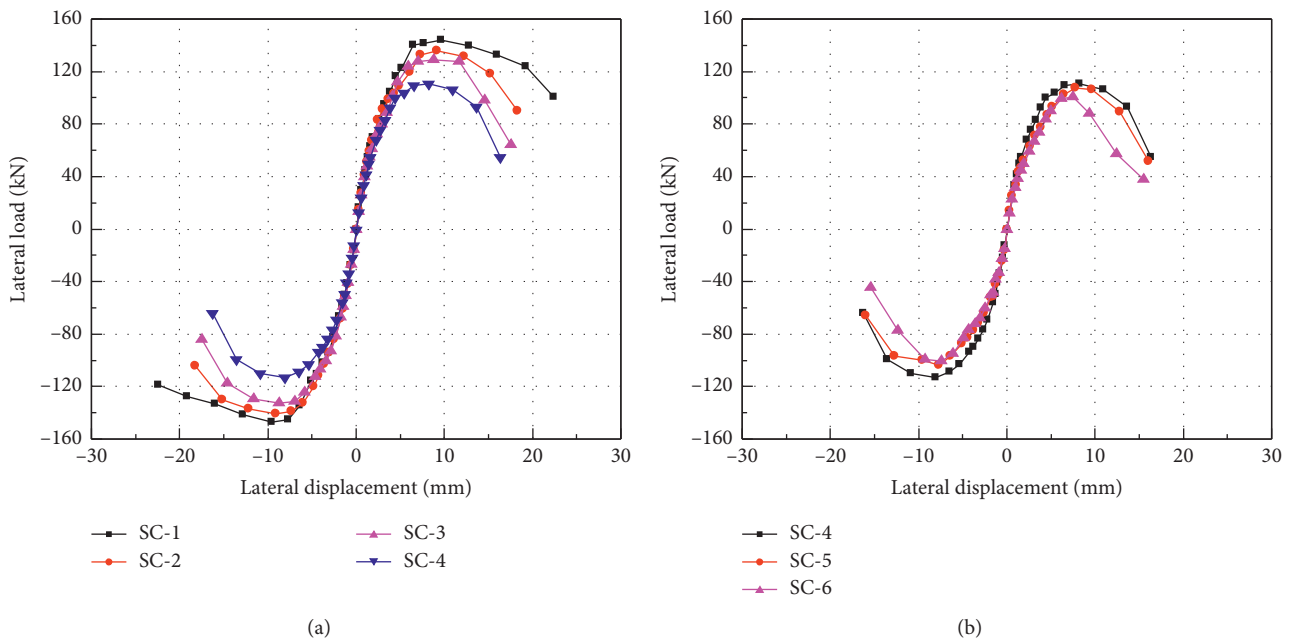

Figure 8: Skeleton curves of the specimens. (a) Corrosion-level-induced changes. (b) Stirrup-ratio-induced changes.

displacement in the positive and negative directions for each displacement-controlled loading level of hysteresis loops.

Based on Figure 8, a number of commonalities in the skeleton curves can be discussed as follows. In the initial stage of loading, the skeleton curves exhibited approximately linear increases. After reaching the yielding point, the curves began to bend, which indicated that the growth rates of the load-carrying capacities for the specimens decreased while the damage to the specimens accumulated. After the peak point, the curves decreased at a rapid pace, which meant the load-carrying capacities of the specimens were greatly reduced. In addition, the positive and negative directions of the skeleton curves were not fully symmetrical, which is likely due to three aspects: (a) the nonsymmetry and discreteness of the corrosion characteristics on the surfaces of steel bars exposed to the artificial climate accelerated corrosion technique, (b) the inevitable deviation during construction and the nonhomogeneity of the concrete material, and (c) the residual deformation that occurred during each level of loading.

Table 6 lists the characteristic parameters of the six column specimens. The yielding points of the specimens were determined by the equivalent energy method. As illustrated in Figure 9, the area of the dashed region *OAB* is equal to that of the dashed region *BCD*: the value, at which the load of a column dropped to 85% of the peak load P_p, was defined as the ultimate load P_u. Based on Figure 8 and Table 6, the following differences existed in the skeleton curves of the specimens under various corrosion levels and stirrup ratios:

(1) In reference to columns SC-1, SC-2, SC-3, and SC-4 with the same stirrup ratios, the loading processes of the noncorroded control specimen and corroded specimens were basically the same under the low cyclic reversed load, which could be categorized into three stages: elastic stage, elastic-plastic stage, and failure stage. Overall, the skeleton curves of the corroded specimens were lower than that of the control specimen. The decreases in the magnitudes of the yielding, peak, and ultimate loads from the control specimen to the corroded specimens displayed the same change rule: each category of these loads was positively correlated with the level of corrosion. For instance, the peak loads of columns SC-2, SC-3, and SC-4 were 4.9, 9.4, and 22.9% less than that of SC-1, respectively. In the elastic stage, the skeleton curves of these four specimens substantially overlapped. In the elastic-plastic stage, the degradation in the load-carrying capacities and lateral stiffnesses of the corroded specimens was more obvious than that of the control specimen. The lengths of the platform segments in the corroded specimens were less than that of the control specimen. After entering the failure stage, the skeleton curves became increasingly steep as the corrosion level increased, which indicated that the load-carrying and deformation capacities of the corroded specimens, compared to the control specimen, were

more severely and more rapidly degraded. Several possible causes exist for the deterioration in the seismic behaviours of the corroded RC column specimens, which was described above. In the first instance, simulated acid rain resulted in the degradation of the mechanical properties of the concrete material [6]. Moreover, compared with a non-corroded steel bar, a corroded steel bar has a lower yield strength, a shorter and less obvious yield platform, and a reduced elongation limit [38]. Lastly, the corrosion product of a steel bar expands in volume, which progressively increases the extrusion force on the surrounding concrete, causing the concrete cover to crack, bulge, and peel off; this phenomenon reduces the bond strength and cooperative working ability among the steel bar and surrounding concrete. These findings illustrate that the impact of acid rain damage on the load-carrying capacity of an RC column is noteworthy.

(2) In reference to columns SC-4, SC-5, and SC-6 with the same corrosion levels, the yielding, peak, and ultimate loads of the specimens were enhanced by increasing the stirrup ratio. As an example, the peak loads of columns SC-4 and SC-5 were 11.3% and 6.5% higher than that of SC-6, respectively. In addition, as the stirrup ratio increased, the length of the platform segments of the skeleton curves correspondingly extended, i.e., the occurrence of the failure working stage was delayed in the specimens. Moreover, the descending branch after the peak points of curves became gentler. Thus, it can be inferred from the above phenomena that increasing the stirrup ratio could fully exert the material properties of concrete in an RC column, thereby efficaciously avoiding the abrupt occurrence of column failure.

4.4. Deformation Capacity. Table 6 shows the deformation parameters of six column specimens, consisting of the yielding, peak, and ultimate displacements corresponding to the yield, peak, and ultimate loads. In addition, the ductility coefficient (μ) and plastic deflection (θ_p) were adopted to assess the ductility variation in an RC column, which is also provided in Table 6 and can be represented as follows:

$$\mu = \frac{\Delta_u}{\Delta_y},$$
$$\theta_p = \frac{\Delta_u - \Delta_y}{L}, \tag{2}$$

where Δ_y and Δ_u are the yielding and ultimate displacements, respectively, and L is the effective length of an RC column specimen.

(1) For columns SC-1, SC-2, SC-3, and SC-4 with the same stirrup ratios, as the corrosion level increased, various deformation parameters of the specimens exhibited downward trends. Specifically, as the

TABLE 6: Main seismic performance parameters of the specimens.

| Specimen	Yielding point		Peak point		Ultimate point		Ductility coefficient μ	Plastic deflection θ_p (rad)
	P_y (kN)	Δ_y (mm)	P_p (kN)	Δ_p (mm)	P_u (kN)	Δ_u (mm)		
SC-1	122.33	5.34	145.53	9.59	123.70	20.60	3.86	0.31
SC-2	116.11	5.03	138.37	9.12	117.61	15.92	3.17	0.22
SC-3	113.53	4.76	131.89	8.73	112.11	14.02	2.95	0.19
SC-4	95.70	4.72	112.22	8.21	95.39	13.52	2.86	0.18
SC-5	89.04	4.70	105.63	7.70	89.79	13.09	2.78	0.17
SC-6	85.26	4.61	100.84	7.43	85.71	10.20	2.21	0.11
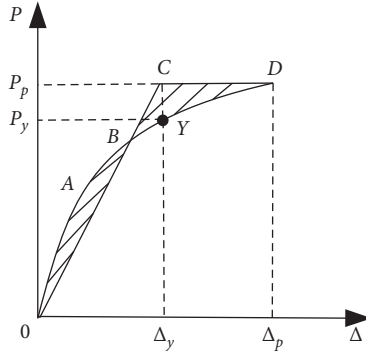
FIGURE 9: Definition of the yielding point.

number of spray cycles increased from 0 to 480, the yielding displacement was reduced from 5.34 to 4.72 mm (11.6%), the peak displacement was reduced from 9.59 to 8.21 mm (14.4%), and the ultimate displacement was reduced from 20.60 to 13.52 mm (34.4%). Furthermore, as the corrosion level increased, a successive reduction was observed in the ductility coefficient and plastic deflection, which illustrated that the deformation capacity of an RC column deteriorated after acid rain exposure. More adversely, the fact that the ductility coefficient of columns SC-3 and SC-4 ranged between 2.86 and 2.95 indicated that these columns exhibited brittle failure modes.

(2) For columns SC-4, SC-5, and SC-6 with the same corrosion levels, the yielding displacement exhibited slight variations from 4.72 to 4.61 mm, which may be because the restraint effect provided by a higher stirrup ratio on the specimens was not obvious during the elastic stage. When the stirrup ratio was increased from A6@100 to A6@60, the peak displacement, ultimate displacement, ductility coefficient, and plastic deflection of the specimens were gradually increased: there was a 10.5% increase in the peak displacement, 32.5% increase in the ultimate displacement, 35.5% increase in the ductility coefficient, and 63.6% increase in the plastic deflection. It can be deduced that increasing the stirrup ratio has a beneficial effect on the ductile deformation capacity of an RC column.

4.5. Stiffness Degradation. The secant stiffness K_i [25] is used to characterize the stiffness values of the specimens, which is calculated according to the following equation:

$$K_i = \frac{|+P_i| + |-P_i|}{|+\Delta_i| + |-\Delta_i|}, \tag{3}$$

where $+P_i$ and $-P_i$ are the maximum load of the first cycle under the i-th displacement-controlled loading level in the positive and negative directions, respectively, and $+\Delta_i$ and $-\Delta_i$ are the displacement values corresponding to $+P_i$ and $-P_i$, respectively.

Based on test data, the secant stiffness values of specimens versus the lateral displacements are calculated using equation (3) and plotted in Figure 10. The observations obtained are summarized as follows:

(1) In terms of generality, the stiffness values of the specimens were originally high. Subsequently, it can be observed that as the loading displacement amplitude increased, the slopes of the stiffness degradation curves were increased, which meant that the stiffness values of specimens were rapidly degraded due to the occurrence and extension of cracks. After the lateral loading displacement reached the displacement value of the peak point, the rate of stiffness degradation decreased and the curve tended to flatten, which might be ascribed to the formation of the dominant diagonal shear cracks in the specimens and the little effect of the generation of secondary cracks on the stiffness.

(2) With respect to columns SC-1, SC-2, SC-3, and SC-4 with the same stirrup ratios and different corrosion levels, the initial stiffness values of the corroded columns were slightly less than that of the noncorroded column. The magnitude of stiffness degradation at the same displacement-controlled loading level was increased by increasing the corrosion level. Moreover, as the loading displacement amplitude increased, the rate of reduction in the stiffness values of the specimens increased with increasing corrosion levels. As shown in Figure 10(a), the curve of column SC-4 had the fastest decreasing rate: These results showed that acid rain has a substantial influence on the stiffness of an RC column.

(3) With respect to columns SC-4, SC-5, and SC-6 with the same corrosion levels and different stirrup ratios, the initial stiffness values of columns SC-4 and SC-5 were 11.5% and 6.2% greater than that of SC-6 at the higher stirrup ratio. As the loading displacement amplitude increased, the degree of degradation in the
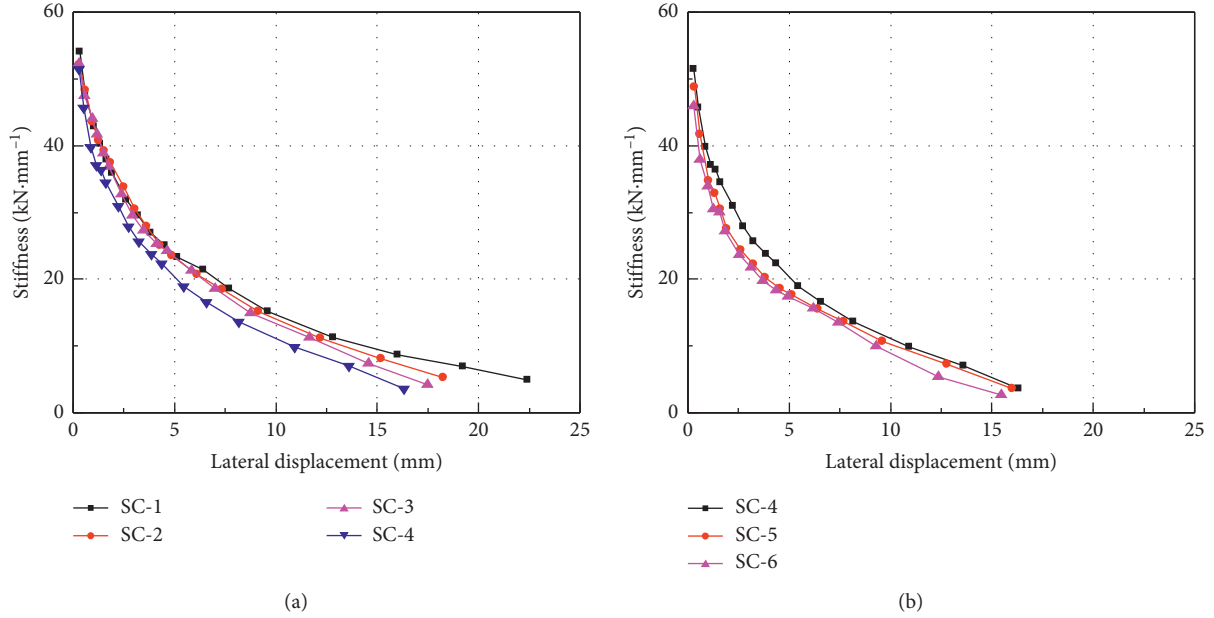
(a)

(b)

FIGURE 10: Stiffness degradation curves of the specimens. (a) Corrosion-level-induced changes. (b) Stirrup-ratio-induced changes.

stiffness values of columns SC-4 and SC-5 was relatively less severe than that of SC-6, i.e., the stiffness of a specimen with a higher stirrup ratio was markedly greater than that of a specimen with a lower stirrup ratio at the same displacement-controlled loading level. This finding shows that increasing the stirrup ratio could improve the resistance-deformation capacity of an RC column to some extent.

4.6. Energy Dissipation Behaviour.
In the seismic design of an RC structure, it is required that the structure and its internal components should have a sufficient energy dissipation capacity so that the structure can consume a substantial amount of seismic energy when subjected to an earthquake without being damaged or immediately collapsing. The cumulative hysteretic dissipation energy E [39] and equivalent viscous damping coefficient h_e [40, 41] are used to evaluate the energy dissipation capacities of the specimens subjected to simulated acid rain exposure.

4.6.1. Equivalent Viscous Damping Coefficient.
The equivalent viscous damping coefficient can be computed from the following equation:

$$h_e = \frac{1}{2\pi} \frac{S_{ABCD}}{S_{\Delta OBE} + S_{\Delta OAD}}, \qquad (4)$$

where S_{ABCD} is the measured area of the hysteresis loop $ABCD$ and $S_{\Delta OBE}$ and $S_{\Delta OAD}$ are the idealized elastic-plastic areas of triangle OBE and OAD, respectively, as shown in Figure 11.

The equivalent viscous damping coefficients h_{ey}, h_{ep}, and h_{eu}, which correspond to yielding, peak, and ultimate points of the specimens, respectively, are summarized in Table 7. As
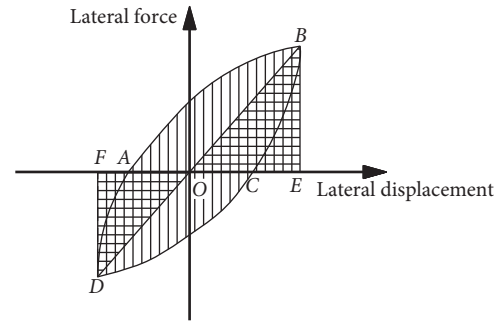

FIGURE 11: Calculation diagram of the equivalent viscous damping coefficient.

TABLE 7: Hysteretic energy dissipation indicators of the specimens.

Specimen	h_{ey}	h_{ep}	h_{eu}	$E \cdot$(kN·mm)
SC-1	0.0556	0.0989	0.1809	11960.50
SC-2	0.0517	0.0879	0.1529	10577.48
SC-3	0.0495	0.0850	0.1517	9338.55
SC-4	0.0425	0.0814	0.1462	7914.72
SC-5	0.0423	0.0679	0.1276	7025.47
SC-6	0.0375	0.0668	0.1205	6473.38

Note: E is the cumulative hysteretic dissipation energy under the thirty-second displacement-controlled loading cycles for easing of comparison, and the total number of loading cycles for the six specimens in Figure 12 is diverse.

shown, (1) with the progression of the loading process in all the specimens, the equivalent viscous damping coefficients gradually increased, indicating that the energy dissipation capacities of specimens were gradually exerted. For columns SC-1 and SC-6, from the yielding points to ultimate points, the equivalent viscous damping coefficients were increased from 0.0556 and 0.0375 to 0.1809 and 0.1205, respectively. (2) A comparison was made among the specimens with the
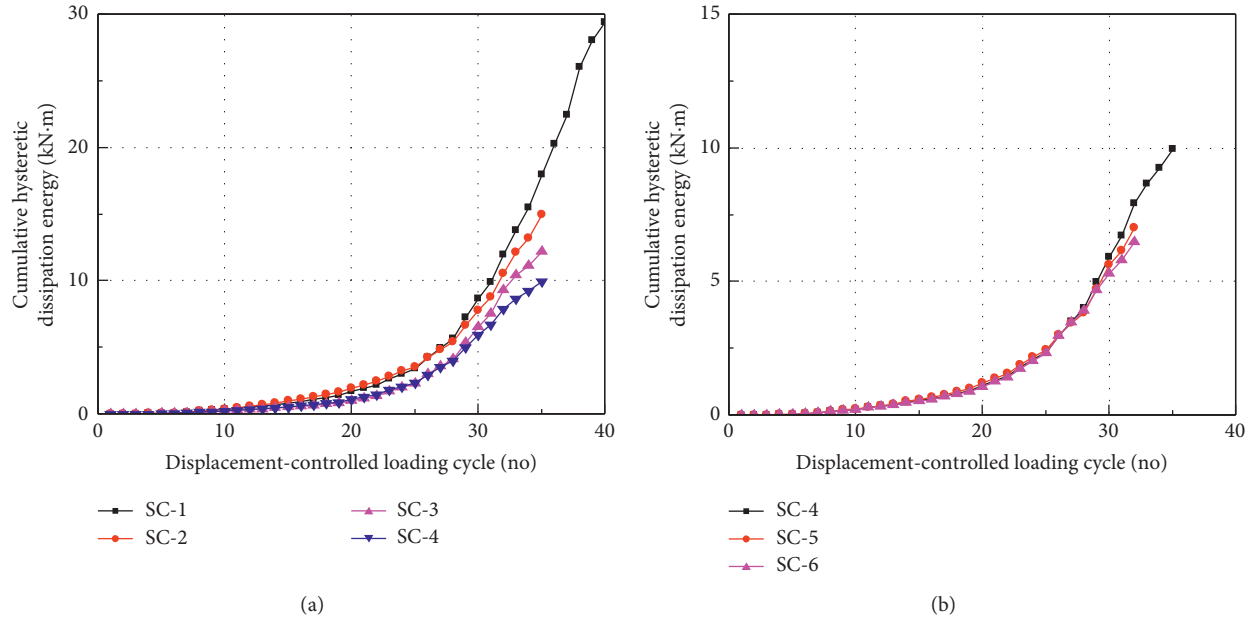
(a)

(b)

FIGURE 12: Cumulative hysteretic dissipation energy curves of the specimens. (a) Corrosion-level-induced changes. (b) Stirrup-ratio-induced changes.

same stirrup ratios (columns SC-1, SC-2, SC-3, and SC-4). The equivalent viscous damping coefficients h_{ey}, h_{ep}, and h_{eu} of the specimens decreased monotonically from 0.0556, 0.0989, and 0.1809 to 0.0425, 0.0814, and 0.1462 as the level of corrosion increased. (3) A comparison among specimens with the same corrosion levels (columns SC-4, SC-5, and SC-6) was also made. As the stirrup ratio increased, the equivalent viscous damping coefficients h_{ey}, h_{ep}, and h_{eu} increased continuously. The equivalent viscous damping coefficients h_{eu} of columns SC-4 and SC-5 were 21.3% and 5.9% greater than that of SC-6, respectively. The above phenomenon showed that the variations in both the corrosion level and stirrup ratio would have significant influences on the fullness of the hysteresis loops of the specimens.

4.6.2. Cumulative Hysteretic Dissipation Energy. One important indicator for quantifying the energy dissipation capacity of an RC column specimen is the cumulative hysteretic dissipation energy, which is the total energy value accumulated under the low cyclic reversed loading test and can be calculated from the following equation:

$$E = \sum_{j=1}^{n} E_j,\tag{5}$$

where E_j is the hysteretic dissipation energy under the j-th displacement-controlled loading cycle and calculated by the measured area of the hysteresis loop *ABCD* as shown in Figure 11, and n is the total number of loading cycles. Figure 12 presents the curves of the cumulative hysteretic dissipation energy of the six column specimens as a function of the displacement-controlled loading cycles. The cumulative hysteretic dissipation energy calculation results for all the specimens are listed in Table 7.

As shown in Figure 12 and Table 7, the cumulative hysteretic dissipation energy values of the specimens were related to three parameters, namely, displacement-controlled loading cycle, corrosion level, and stirrup ratio, as specifically described below. (1) As the displacement-controlled loading cycle increased, the total dissipated energy values of all specimens increased monotonically during the loading tests. (2) In reference to columns SC-1, SC-2, SC-3, and SC-4 with the same stirrup ratios, obvious reductions were observed in the cumulative hysteretic dissipation energy of specimens subjected to simulated acid rain exposure, and the magnitudes of these reductions were increased by increasing the corrosion level. The cumulative energy values of the corroded columns SC-2, SC-3, and SC-4 were 11.5, 21.9, and 33.8% less than that of the control column SC-1, respectively. Moreover, as the number of displacement-controlled loading cycles increased, the difference in the cumulative hysteretic dissipation energy values between the noncorroded and corroded specimens gradually increased. This finding suggests that the energy dissipation capacity of an RC column is substantially affected by the corrosion level. (3) In reference to columns SC-4, SC-5, and SC-6 with the same corrosion levels, the cumulative hysteretic dissipation energy values of the specimens were increased in stages as the stirrup ratio increased. The cumulative energy values of columns SC-4 and SC-5 significantly increased: these values were 22.3% and 8.5% greater than that of SC-6, respectively. This finding indicates that increasing the stirrup ratio can enhance the energy dissipation capacity of an RC column.

5. Conclusions

This paper conducted a sequence of artificial climate accelerated corrosion tests and low cyclic reversed loading tests on six RC column specimens. The influences of the corrosion level and stirrup ratio on the visual damage, failure mode, and various seismic behaviour indexes of the columns were systematically investigated. On the basis of the primary test results, the following conclusions can be drawn:

(1) The appearance characteristics of the six column specimens exhibited varying degrees of visual damage from the simulated acid rain exposure. The greater the level of corrosion, the more severe the visual damage of the specimens. For column SC-4, which was subjected to 480 spray cycles, the surface became rough and pitted, some of the coarse aggregates were exposed, and the concrete texture loosened.

(2) All six column specimens were dominated by analogous flexural-shear failures under the low cyclic reversed loads, despite the distinctions in corrosion level and stirrup ratio. Nevertheless, there were some variations in the damage processes of the specimens with different corrosion levels and stirrup ratios. With increasing levels of corrosion, the number of cracks in the lower parts of the columns decreased, whereas the crack spacing increased and the crack width broadened. As the stirrup ratio increased, X-shaped flexural-shear cracks in the plastic hinge areas of the columns occurred later in the loading process, and the propagation speed of these cracks was slower. Furthermore, the pinching effect of the hysteresis loops became increasingly obvious.

(3) In regard to the specimens with the same stirrup ratios, as the corrosion level increased, the load-carrying capacities, deformation capacities, stiffnesses, and energy dissipation capacities of the specimens were continuously decreased. Compared with the control column SC-1, the peak load, ductility coefficient, and cumulative hysteretic dissipation energy of the highly corroded column SC-4 decreased by 22.9, 25.9, and 33.8%, respectively.

(4) Regarding the specimens with the same corrosion levels, the higher the stirrup ratio, the stronger the restraint effect of the stirrups on the concrete, and the seismic behaviours of the specimens were obviously improved. The peak load, ductility coefficient, initial stiffness, and cumulative hysteretic dissipation energy of column SC-4 were 11.3, 35.5, 11.5, and 22.3% greater than those of SC-6.

Data Availability

The data used to support the findings of this paper are available from the corresponding author upon request.

Conflicts of Interest

The authors declare that there are no conflicts of interest regarding the publication of this paper.

References

[1] Y.-Z. Cao, S. Wang, G. Zhang, J. Luo, and S. Lu, "Chemical characteristics of wet precipitation at an urban site of Guangzhou, South China," *Atmospheric Research*, vol. 94, no. 3, pp. 462–469, 2009.

[2] P. C. Mouli, S. V. Mohan, and S. J. Reddy, "Rainwater chemistry at a regional representative urban site: influence of terrestrial sources on ionic composition," *Atmospheric Environment*, vol. 39, no. 6, pp. 999–1008, 2005.

[3] F. C. Menz and H. M. Seip, "Acid rain in Europe and the United States: an update," *Environmental Science & Policy*, vol. 7, no. 4, pp. 253–265, 2004.

[4] D.-J. Ling, Q.-C. Huang, and Y. Ouyang, "Impacts of simulated acid rain on soil enzyme activities in a latosol," *Ecotoxicology and Environmental Safety*, vol. 73, no. 8, pp. 1914–1918, 2010.

[5] Y. Lv, C. Wang, Y. Jia et al., "Effects of sulfuric, nitric, and mixed acid rain on litter decomposition, soil microbial biomass, and enzyme activities in subtropical forests of China," *Applied Soil Ecology*, vol. 79, pp. 1–9, 2014.

[6] Y. F. Fan, Z. Q. Hu, Y. Z. Zhang, and J. L. Liu, "Deterioration of compressive property of concrete under simulated acid rain environment," *Construction and Building Materials*, vol. 24, no. 10, pp. 1975–1983, 2010.

[7] V. Zivica and A. Bajza, "Acidic attack of cement based materials-a review: part 1. Principle of acidic attack," *Construction and Building Materials*, vol. 15, no. 8, pp. 331–340, 2001.

[8] Y. Y. Guan and S. S. Zheng, "Seismic behaviors of RC frame beam-column joints under acid rain circle: a pilot experimental study," *Journal of Earthquake Engineering*, vol. 6, no. 22, pp. 1–19, 2017.

[9] J. Hill, E. A. Byars, J. H. Sharp, C. J. Lynsdale, J. C. Cripps, and Q. Zhou, "An experimental study of combined acid and sulfate attack of concrete," *Cement and Concrete Composites*, vol. 25, no. 8, pp. 997–1003, 2003.

[10] M. Gregerová and D. Všianský, "Identification of concrete deteriorating minerals by polarizing and scanning electron microscopy," *Materials Characterization*, vol. 60, no. 7, pp. 680–685, 2009.

[11] S. Xie, L. Qi, and D. Zhou, "Investigation of the effects of acid rain on the deterioration of cement concrete using accelerated tests established in laboratory," *Atmospheric Environment*, vol. 38, no. 27, pp. 4457–4466, 2004.

[12] M.-C. Chen, K. Wang, and L. Xie, "Deterioration mechanism of cementitious materials under acid rain attack," *Engineering Failure Analysis*, vol. 27, pp. 272–285, 2013.

[13] H. Okochi, H. Kameda, S.-I. Hasegawa, N. Saito, K. Kubota, and M. Igawa, "Deterioration of concrete structures by acid deposition-an assessment of the role of rainwater on deterioration by laboratory and field exposure experiments using mortar specimens," *Atmospheric Environment*, vol. 34, no. 18, pp. 2937–2945, 2000.

[14] X. X. Zha and J. K. Lu, "Study of durability of recycled concrete under the environment of the acid rain," *Applied Mechanics and Materials*, vol. 71–78, pp. 5042–5045, 2011.

[15] Z. Wang, Z. Zhu, X. Sun, and X. Wang, "Deterioration of fracture toughness of concrete under acid rain environment," *Engineering Failure Analysis*, vol. 77, pp. 76–84, 2017.

[16] C. Zhou, Z. Zhu, Z. Wang, and H. Qiu, "Deterioration of concrete fracture toughness and elastic modulus under simulated acid-sulfate environment," *Construction and Building Materials*, vol. 176, pp. 490–499, 2018.

[17] Y. F. Fan, D. W. Wang, and H. Y. Luan, "Study on the load carrying capacity of reinforced concrete beams under acid precipitation," *Engineering Mechanics*, vol. 31, no. 4, pp. 147–154, 2014, in Chinese.

[18] A. C. Lynn, J. P. Moehle, S. A. Mahin, and W. T. Holmes, "Seismic evaluation of existing reinforced concrete building columns," *Earthquake Spectra*, vol. 12, no. 4, pp. 715–739, 1996.

[19] N. S. Vu and B. Li, "Seismic performance assessment of corroded reinforced concrete short columns," *Journal of Structural Engineering*, vol. 144, no. 4, Article ID 04018018, 2018.

[20] Y. Ma, Y. Che, and J. Gong, "Behavior of corrosion damaged circular reinforced concrete columns under cyclic loading," *Construction and Building Materials*, vol. 29, pp. 548–556, 2012.

[21] D. Li, R. Wei, F. Xing, L. Sui, Y. Zhou, and W. Wang, "Influence of non-uniform corrosion of steel bars on the seismic behavior of reinforced concrete columns," *Construction and Building Materials*, vol. 167, pp. 20–32, 2018.

[22] A. Meda, S. Mostosi, Z. Rinaldi, and P. Riva, "Experimental evaluation of the corrosion influence on the cyclic behaviour of RC columns," *Engineering Structures*, vol. 76, pp. 112–123, 2014.

[23] Q. Li, D.-T. Niu, Q.-H. Xiao, X. Guan, and S.-J. Chen, "Experimental study on seismic behaviors of concrete columns confined by corroded stirrups and lateral strength prediction," *Construction and Building Materials*, vol. 162, pp. 704–713, 2018.

[24] S.-Y. Yang, X.-B. Song, H.-X. Jia, X. Chen, and X.-L. Liu, "Experimental research on hysteretic behaviors of corroded reinforced concrete columns with different maximum amounts of corrosion of rebar," *Construction and Building Materials*, vol. 121, pp. 319–327, 2016.

[25] JGJ 101-96, *Specificating of Testing Methods for Earthquake Resistant Building*, China Architecture & Building Press, Beijing, China, 1996, in Chinese.

[26] GB 50010-2010, *Code for Design of Concrete Structures*, China Architecture & Building Press, Beijing, China, 2010, in Chinese.

[27] GB 50011-2010, *Code for Seismic Design of Buildings*, China Architecture & Building Press, Beijing, China, 2010, in Chinese.

[28] W. Yang, S.-S. Zheng, D.-Y. Zhang, L.-F. Sun, and C.-L. Gan, "Seismic behaviors of squat reinforced concrete shear walls under freeze-thaw cycles: a pilot experimental study," *Engineering Structures*, vol. 124, pp. 49–63, 2016.

[29] Q. Qin, S. Zheng, L. Li, L. Dong, Y. Zhang, and S. Ding, "Experimental study and numerical simulation of seismic behavior for RC columns subjected to freeze-thaw cycles," *Advances in Materials Science and Engineering*, vol. 2017, Article ID 7496345, 13 pages, 2017.

[30] S. Xu, A. Li, Z. Ji, and Y. Wang, "Seismic performance of reinforced concrete columns after freeze-thaw cycles," *Construction and Building Materials*, vol. 102, pp. 861–871, 2016.

[31] Bulletin of the State of the Environment of China, 2016, http://www.mee.gov.cn/hjzl/.

[32] H. B. Hu, "Analysis for simulation test on acid rain attacking concrete," *Journal of the Chinese Ceramic Society*, vol. 36, no. S1, pp. 147–152, 2008, in Chinese.

[33] S. D. Xie, D. Zhou, Q. X. Yue, and H. L. Liu, "Study of simulated acid rain on concrete," *Environmental Science*, vol. 16, no. 5, pp. 22–26, 1995, in Chinese.

[34] Q. Q. Zhang, Y. Yan, Z. F. Wang, and X. N. Dong, "Precipitation characteristics in chongqing during 1961–2012," *Journal of Nanjing University of Information Science & Technology (Natural Science Edition)*, vol. 8, no. 3, pp. 215–225, 2016, in Chinese.

[35] T. Paulay and M. J. N. Priestley, *Seismic Design of Reinforced Concrete and Masonry Buildings*, pp. 140–142, John Wiley & Sons, Hoboken, NJ, USA, 1992.

[36] J. G. Niu, H. T. Zhai, and D. T. Niu, "Investigation on neutralization rules of concrete under loads subjected to acid rain attack," *Advanced Materials Research*, vol. 243–249, pp. 5768–5771, 2011.

[37] B. Li, L. Cai, and W. Zhu, "Predicting service life of concrete structure exposed to sulfuric acid environment by grey system theory," *International Journal of Civil Engineering*, vol. 16, no. 9, pp. 1017–1027, 2018.

[38] Q. Wu and Y. S. Yuan, "Experimental study on the deterioration of mechanical properties of corroded steel bars," *China Civil Engineering Journal*, vol. 41, no. 12, pp. 42–47, 2008, in Chinese.

[39] C. Qian, Y. Li, D. Xie, N. Li, and X. Wen, "Seismic performance experiment involving one-story, two-bay self-control energy dissipation UPPC frames under low cyclic loads," *Ksce Journal of Civil Engineering*, vol. 23, no. 7, pp. 3041–3048, 2019.

[40] Z. Zhu and Z. Guo, "Seismic behavior of precast concrete shear walls with different confined boundary elements," *Ksce Journal of Civil Engineering*, vol. 23, no. 2, pp. 711–718, 2019.

[41] H. Zhang, H. Liu, G. Li, and X. Ning, "Seismic performance of encased steel plate-reinforced gangue concrete composite shear walls," *Ksce Journal of Civil Engineering*, vol. 23, no. 7, pp. 2919–2932, 2019.